CrossMark

Microfluidic Mimic for Colloid Membrane Filtration: A Review

Nandini Debnath[1] and Mohtada Sadrzadeh[2]* ⓘ

Abstract | This review provides an overview of the recent improvements of microfluidic membrane mimics. A special focus is given to the filtration of colloids in this device. Methods for on-chip membrane filtration have undergone significant development and improvement over the past two decades. Many efforts have been made to develop a single chip microfluidic platform that integrates the benefits of microfluidics and membrane science and technology. This review addresses the potential for microfluidic devices to serve as microfiltration membranes for separation purposes, as well as, micro-sized tools to study colloidal fouling phenomena at the pore scale.

1 Introduction

A globally sustainable supply of clean, fresh water is necessary to human life and food supply, industrial processes, and energy production[1]. Traditional clean water sources are limited, and their pollution due to the rapid urbanization and industrialization calls for a more effective, low-cost, robust water treatment processes[2].

Membrane separation processes have become one of the fastest emerging technologies. For water treatment, membranes are essential due to their distinct advantages over traditional processes, primarily lower operating costs, compact design, and high product quality[3]. Advanced membranes provide a potential solution for water and energy sustainability[4, 5]. The main advantage of membranes is that they can be used for recovery and purification of a huge variety of materials across broad range industries[6, 7]. There are various types of pressure-driven liquid-based membrane processes applicable for water treatment including microfiltration (MF), ultrafiltration (UF), nanofiltration (NF) and reverse osmosis (RO). They can be categorized by their pore sizes: MF is the most porous and RO is the densest one. NF and RO membrane are used for water desalination and softening while MF and UF are mainly utilized for removing suspended solids, colloids, pathogens, emulsions from contaminated water sources[7].

A major challenge for the sustainable use of membrane filtration processes is fouling of membranes by the attachment of water contaminants (colloidal particles, organic matter, and biomaterials) onto their surfaces. Fouling has several negative impacts on filtration such as reducing water flux and salt rejection, increasing the cleaning demand, and decreasing the life cycle of membranes and subsequently increasing the operating cost of the water treatment process. The reduction of membrane performance due to the adsorption of colloidal particles on the surface or within the membrane pores is the most common challenge in MF/UF processes[8, 9]. Colloidal particles reduce the membrane performance by the development of a concentration polarization layer and formation of a cake fouling layer on the membrane surface[10]. To overcome this challenge, a membrane module is typically considered as an opaque system, where only the input and the output can be measured and analyzed. Further, a microfluidic device can be utilized to visualize and understand the fluid flow at pore scale, investigate the nature, properties, and evolution of colloidal fouling.

A microfluidic chip is a pattern of the engraved microchannel through which fluids are directed, mixed and separated. Advancement in the microfabrication technology has enabled the development of microfluidics for diverse applications like lab-on-a-chip[11, 12], nanoparticle separation[13–15], chemical sensors[16, 17], detection of pathogens[17], electrophoresis[18, 19], micro-nozzles[20], microvalves[21, 22], and DNA analysis[23, 24].

[1] Department of Mechanical Engineering, 6-074 National Institute for Nanotechnology (NINT), Advanced Water Research Lab (AWRL), University of Alberta, Edmonton, AB T6G 1H9, Canada.
[2] Department of Mechanical Engineering, 10-367 Donadeo Innovation Centre for Engineering, 6-074 National Institute for Nanotechnology (NINT), Advanced Water Research Lab (AWRL), University of Alberta, Edmonton, AB T6G 1H9, Canada.
*sadrzade@ualberta.ca

Springer IISc Press

Microfluidic chips can be designed to mimic the pore sizes of various membranes (0.1–10 μm for MF) filtration operating modes (dead-end or cross-flow). A microfluidic membrane mimic system, where inertia (Re ≪ 1 or stokes number ≪ 1) is negligible, can be reasonable to simulate an MF process[25]. It can provide a legitimate strategy to simulate the fluid flow in conventional membrane filtration processes[26, 27]. For microfluidic membranes, transport is mostly governed by membrane pore size and is not an intrinsic material property, although interaction with the internal membrane surface can play a crucial role. The primary advantage of a microfluidic membrane mimic is the easy parallel experimentation, ability to collect large amounts of data, real-time observation of transport phenomena and evolution of the fouling inside the system through microscopy. Connecting the membrane to a microfluidic chip also allows for the optimization of separation process and mitigation of fouling at the pore scale. However, there are critical gaps between traditional filtration systems and microfluidic filtration systems. As the modern technology evolves, these gaps can be bridged with microfluidic membrane mimic systems.

In this paper, first, the theoretical basis of microfluidics, membranes and colloid filtration is presented. Next, the fabrication methods for microfluidic membrane mimics are discussed. Then, the scope of microfluidic colloid filtration in microfluidic membrane mimic filtration systems is presented. Finally, the advantages and limitations of microfluidic membranes mimic for colloid filtration are discussed, and future opportunities are provided.

2 Theory

2.1 Fundamentals of Microfluidics
Microfluidics refers to the precise control, manipulation, and multiplexing of fluid at the micron scale in at least one dimension. With this miniaturization, microfluidics enables analyzing fluid flow for conventional laboratory processes on a single chip. The main advantage of microfluidics is the increased ratio of surface-to-volume with improved performance, including rapid sample processing, high integrity, low reagent consumption, and precise fluid control.

However, microfluidic devices suffer from several limitations[28, 29]. It is important to note that these devices are sensitive to surface physical and chemical properties[12, 29]. At the micro level, the microfluidic fluid behavior can be affected by several factors such as surface tension, laminar flow

effect, capillary, energy dissipation, and fluidic resistance[12, 30]. More about fabrication techniques of microfluidic devices can be found in several reviews[11, 14, 31, 32]. The common material used for the fabrication of microfluidics are silicon, silica, metal, glass, polymer (PDMS) and paper[33].

Modelling fluid flow in microfluidics is generally performed using continuum theory[34]. This is because the smallest feature size that can be patterned using microfabrication is limited by the diffraction of light to 0.5 μm for contact photolithography[35], which is much larger than the mean free path of molecules. Hence, for an incompressible Newtonian fluid, the flow is defined by the Navier–Stokes and continuity equations as follows,

$$\rho \frac{\partial u}{\partial t} + \rho(u \cdot \nabla)u = f_b - \nabla P + \mu \nabla^2 u \quad (1)$$

$$\nabla \cdot u = 0 \quad (2)$$

where u is the velocity vector, ρ is the density of the fluid, P is the pressure, t is time, μ is dynamic viscosity, and f_b is the body force. Here, the inertial acceleration term appears on the left and forces are on the right. For a concentration distribution, the convection–diffusion equation is applied as follows,

$$\frac{\partial c}{\partial t} + (u \cdot \nabla)c = D\nabla^2 c \quad (3)$$

where c is the concentration and D is the diffusion coefficient. For a microfluidic flow, often the magnitude of inertial and viscous forces are compared with non-dimensional Reynolds number ($Re = \rho u l / \mu$, where l is the characteristic length). Another non-dimensional number, the Peclet number ($Pe = lu/D$), is used to determine the ratio of convective and diffusive transport.

2.2 Fundamentals of Membrane Processes
A membrane is a semi-permeable barrier that allows the selective removal of particles, molecules, or ions from a solution[7]. The transport of molecules through the membrane occurs due to the chemical potential difference between the two phases. In general, the membrane performance is characterized by permeate flux and salt rejection. In a pressure-driven porous membrane, the permeate flux (J) is governed by the pore flow model and is typically expressed by the Hagen–Poiseuille equation as follows,

$$J = \frac{\varepsilon r^2}{8\mu\tau} \frac{\Delta P}{\Delta t} \quad (4)$$

where J is the flux per unit area, ΔP is the pressure difference and Δt is the membrane thickness, ε is the porosity, τ is the tortuosity, μ is the viscosity, and r is the radius of a pore. For a dense membrane, however, the transport phenomenon is governed by solution–diffusion mechanism and is an intrinsic property of the membrane material. The relationship between the diffusion coefficient, D, the permeability, P, and solubility coefficient, S, can be given by

$$P = D \cdot S. \tag{5}$$

In a porous membrane, the transport is controlled by the membrane morphology, not the intrinsic material property. Membrane morphology is characterized by the porosity (ε) and tortuosity (τ). The porosity (ε) is a measure of the fraction of the empty spaces to the total volume, or surface, which ranges <0.02 for nanometer-sized pore and >0.82 for micrometer-sized pores (considering pore size range from 1 nm to 10 μm). The tortuosity (τ) is a measure of the average path length through a pore across the thickness of the membrane. Retention, R, is defined as an alternative to selectivity. Retention ranges from 0%, indicating no contaminant rejection by the membrane to 100%, indicating complete restriction to pass through membrane pores. Retention depends on the ratio of contaminant size to pore size and is expressed as,

$$R = 1 - \frac{c_p}{c_f} \tag{6}$$

where c_p and c_f are the concentrations of contaminants in the permeate and feed, respectively. A combination of water recovery (permeability P) and water quality (retention) provides an idea of a membrane separation performance.

2.3 Fundamentals of Colloid Filtration

Colloids are microscopically dispersed, insoluble, suspended particles whose characteristic size in at least one spatial direction is between 1 nm and 1 μm[36]. Colloids include a broad range of materials including particles, surfactants, and polymers and can be of three distinct phases (solid, liquid and gas), depending on the dispersed phase and dispersion media. In colloid membrane filtration, critical flux is defined as the permeate flux above which irreversible colloidal fouling occurs. At the beginning of filtration, critical flux is governed by a balance between drag force and colloid–surface interactions. Over time, colloid–colloid interactions also come to play. However, the dispersion stability and the fouling scenario may vary at the

pore scale. Besides these two types of interactions (colloid–surface and colloid–colloid), at the pore scale, critical flux can be influenced by hydrodynamic effects, the local morphologies, and the topography of the membrane surface[37].

To understand the process of particle capture on the membrane surface in colloid membrane filtration, surface interactions must be understood. Experimental observations with various colloidal dispersions have shown that colloidal stability due to colloid–surface interaction varies the permeate flux. Yao et al.[38] suggested a classical colloid filtration theory (CFT) to describe the filtration of colloidal particles. In this model, the removal of colloidal particles by a membrane is considered to follow a first-order kinetics, causing an exponential decline of colloidal concentration from the surface to the bulk. Tufenkji et al.[39] showed the deviation from the CFT in the light of DLVO (Derjaguin, Landau, Verwey, and Overbeek) theory. Their experimental study suggested that secondary energy minimum and surface charge heterogeneities played critical roles in significant deviation from CFT. Observation of these phenomena is very important to understand fouling behavior and the formation mechanism of a cake layer. A growing body of experimental research suggests that the deposition behavior of microbial particles (e.g., bacteria and virus) is inconsistent with the classical CFT. These results have important implications for the prediction of colloidal and microbial transport and their interactions in natural and engineered systems[39,40].

Theoretically, the surface interaction for colloid filtration is generalized into two categories: colloid–surface interaction and colloid–colloid interaction[37]. Colloid–surface interaction can be expressed by a net flux (J_{cs}), which is a balance between the convective term and a diffusive term for a single particle–surface interaction and is given by

$$J_{cs} = J\phi - D\frac{d\phi}{dz} - \frac{D}{kT}\phi\frac{dV}{dz}. \tag{7}$$

here ϕ is the colloid volume fraction, k is the Boltzmann constant, T is the absolute temperature and V is the colloid–surface interaction potential. The first term on the right-hand side is convective transport; the second term indicates diffusive transport and the third term shows the relocation of colloids to the membrane surface, due to surface interactions. The third term can be positive or negative, respectively, depending on the attractive or repulsive surface interaction potential. A schematic representation of a single particle interacting with surface and

J. Indian Inst. Sci. |VOL 98:2|137–157 June 2018|journal.iisc.ernet.in

Springer   IISc Press

139

corresponding critical operating conditions for the deposited state is given in Fig. 1a[37].

A critical permeation flux (J_{cr}) can be defined by obtaining a balance between the convective term (drag force) and the repulsive interaction between the colloid and the surface. The critical flux (J_{cr}) can be calculated from the continuity equation and the DLVO potential interaction and can be linked to the critical Peclet number (Pe_{cr}) as follows[41]

$$J_{cr} = \frac{D}{\delta} P_{cr} \qquad (8)$$

$$P_{cr} = \ln\left(\frac{V_{cs}}{\delta}\right) \qquad (9)$$

where δ is the mass boundary layer thickness which depends on the fluid velocity, u. V_{cs} is the potential barrier for the colloid–surface interactions expressed in terms of the colloid–surface interaction potential, V, as,

$$V_{cs} = \int_0^\infty \left(e^{\frac{V}{kT}} - 1\right) dz \qquad (10)$$

A critical Peclet number (Pe_{cr}) can be defined above which a solid phase transition occurs. For many-body colloid–colloid interactions, the net flux (J_{cc}) towards the membrane surface can be expressed as,

$$J_{cc} = J\phi - D(\phi, V)\frac{d\phi}{dz} = J\phi - \frac{K(\phi)}{6\pi\mu a}V_c\frac{d\prod}{dz} \qquad (11)$$

where V denotes now colloid–colloid interaction potential, V_c is the spherical colloid volume, a is the spherical colloid radius, $K(\phi)$ is the

settling hindrance coefficient [$K(\phi) = m/m_0$, m is the mobility] and $\prod$ is the osmotic pressure. The second term on the right-hand side represents the many-body colloid–colloid interactions. The modified diffusion coefficient $D(\phi, V)$ can further be expressed in terms of the gradient of osmotic pressure via Stokes–Einstein relationship[37, 41, 42]. In this case, a transition to a solid state occurs when the concentration is high enough that the attraction between colloid–surface overcomes the dispersive force. A schematic representation of the many-body colloid–colloid interactions with membrane surface, and critical condition for solid state, is shown in Fig. 1b[37]. In a cross-flow filtration, the Pe_{cr} can be expressed as[37]

$$Pe_{cr(cf)} = \frac{J\delta}{D_0} = \frac{V_c}{kT}\int_{\prod_b}^{\prod_{cr}}\frac{K(\phi)}{\phi}d\prod \qquad (12)$$

which depends on the permeate flux, as well as, the thickness of the boundary layer, δ. In dead-end filtration, the Pe_{cr} depends on both the permeate flux and the accumulated mass of colloids, V_a (proportional to filtered volume), which is expressed as[37]

$$Pe_{cr(de)} = \frac{JV_a}{D_0} = \frac{V_c}{kT}\int_{\prod_b}^{\prod_{cr}}K(\phi)d\prod \qquad (13)$$

In summary, when analyzing the critical flux, one can decipher the formation of a fouling layer on the membrane surface by considering the influence of the hydrodynamics and the colloid–surface, and colloid–colloid interactions at
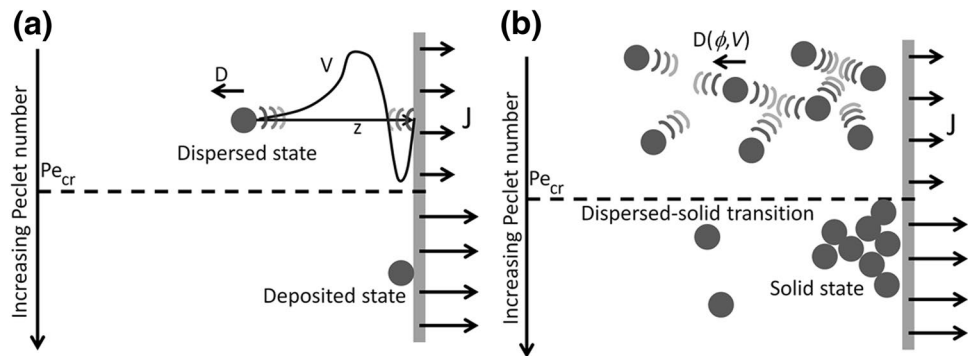

Figure 1: a Colloid–surface interaction: a schematic of the representation of a single particle interacting with membrane surface and the corresponding critical condition is given for a deposited state. **b** Colloid–colloid interactions: a schematic of the representation of many-body colloid–colloid interactions and the corresponding critical operating condition is given for a transition from dispersed state to solid state[37]. (Copyright 2011, reproduced with permission from Elsevier).

140

Springer IISc Press

J. Indian Inst. Sci.|VOL 98:2|137–157 June 2018|journal.iisc.ernet.in

the pore scale. Thus, developing an experimental method with the in situ device would improve our understanding of colloidal fouling.

3 Microfluidic Membrane On-chip

In this section, a particular focus is placed on the methodology to bridge membrane technology and microfluidics. Different fabrication techniques, e.g., photolithography, soft lithography, hot embossing, micromachining, wet etching, dry etching, deep reactive ion etching (DRIE), injection molding, and E-beam lithography have been used so far. A broader discussion about the fabrication of microfluidic membrane devices can be found in several reviews[25–27]. These methods can be divided into three major categories: (1) production of sieves; (2) production of an array of pillars or structures; and (3) membrane-less filtration. Table 1 summarizes some of the different approaches within these three categories.

The fabricated microfluidic membrane filtration devices by sieve and pillar method have been broadly used for biological and medical applications[47, 56, 57, 65, 89], fouling investigations[37, 48, 80, 83, 90, 109], chemical reagent detection[65], sample pretreatment[60], oil–water separation[57, 92], removal of macromolecules and aggregates[13, 15, 82, 85, 93], removal of solutes such as protein[59, 80], microreactor research[58, 73], DNA separation[24, 75, 80], controlled drug delivery[61, 64, 75], and pervaporation and gas separation[46, 50, 52, 110].

3.1 Production of Sieves

To produce sieves, the first, simple, easy and sophisticated way of fabricating microfluidic membrane mimic devices is to insert a membrane with the required pore size on to a chip. Second approach is the direct casting of sieves made of a permeable membrane where transverse and lateral filtration take place as the particle can pass through the membrane pores and fabricated sieves. Third approach is the direct casting of sieves made of an impermeable membrane where transverse filtration takes place as the particles can pass through sieves only. For these three kinds, different materials, such as PDMS[14, 15, 49–52] and other polymeric materials[43, 55, 60–63], hydrogel[66, 67], paper[76], Si[68–70], zeolite[71–73], and alumina[74, 75], can be used. In a pressure-driven membrane filtration device, the dead-end or cross-flow MF membrane can be fabricated with various sieve sizes (0.1–10 μm) through which the feed solution can pass while components larger than the sieve size are retained. It is important to note that, to explore membrane properties, only the membrane mimic pore size area can be treated as a membrane surface area (excluding microfluidic channel).

3.1.1 Insertion of Membrane/Sieve On-Chip
The most straightforward method of creating an effective and low-cost microfluidic membrane mimic is to integrate a membrane on-chip to a

Table 1: Summary of different approaches for microfluidic membrane mimics on-chip.

Methods	Approaches	Filtration mode	Materials
Production of sieves	Insertion of membrane/ sieve on chip-sandwiched method[26, 43–48]	Dead-end and cross flow filtration	PDMS chip[14, 15, 47–59] Other polymeric chip[24, 43, 55, 60–65]
	Direct casting of sieves made of permeable membrane[68, 70, 77–79]		Hydrogel based chip[66, 67] Glass[60] Silicon and silica[68–70] Zeolite[71–73] Alumina[74, 75] paper[76] etc.
	Direct casting of sieves made of impermeable membrane[61, 80, 81]		
Production of an array of pillars or structures	Pillars or structures made of impermeable membrane materials[13, 15, 22, 37, 49, 50, 82–93]	Dead-end filtration	PDMS chip[13, 15, 37, 49, 50, 82–93] Glass[91] Teflon chip[22]
Membrane-less filtration	Inertial transport and solute gradient[94–96]	Dead-end and cross flow filtration	PDMS chip[94–97]
	Liquid membrane formation[98–101]		PDMS chip[98] Glass[92–94]
	Lipid membrane formation[102–108]		PDMS chip[97–99] Other polymeric chip[101, 102], Mica and SiO$_2$[102, 107] Si$_3$N$_4$[103]

traditional membrane by clamping or gluing[26]. In the most common approach, an initial pattern is defined on a Si/glass wafer by lithography. After that, wet etching (using KOH or tetramethylammonium hydroxide solution) or dry etching (using Reactive Ion Etching, RIE or Deep Reactive Ion Etching, DRIE) is performed following a proper recipe to etch the small features and micro-channels. Lastly, a micro-patterned layer is bonded to a flat surface (glass) using either an adhesive or a plasma bonding method to complete the microfluidic membrane assembly. This is best known as the sandwiched method. The assembled device allows having a "top view" of the pores for microscopic visualization. Di et al.[44] studied a microfluidic system for particle deposition during UF of KCl solutions containing 0.4 μm (mean diameter) latex suspensions. Direct visualization of the deposition of particles onto the membrane surface was possible when they sandwiched PES membrane between a PDMS layer and a Si substrate (Fig. 2a). Cheng et al.[43] innovated a multilayer-filtration method by incorporating cyclopore polycarbonate (PC) membranes (with a pore size of 3 μm) on an adhesive layer, which was fixed on a bottom fluidic channel layer made of polymethyl methacrylate (PMMA). Next, a 120 μm thick

PDMS layer and porous polytetrafluoroethylene (PTFE) membranes (with a pore size of 0.2 μm) were assembled with top fluidic channels in a sequence, as shown in Fig. 2b.

Liang et al.[111] developed an integrated double-filtration microfluidic device for the separation, enrichment, and quantification of urinary extracellular vesicles for the detection of bladder cancer. The primary and secondary filtration processes consisted of 200 nm and 30 nm pore size membranes integrated along the cross-section of a microfluidic channel (Fig. 2c). Insertion of porous membrane on-chip was not only limited to liquid flow but also used for pervaporation and gas separation[46].

3.1.2 Direct Casting of Sieves Made of a Permeable Membrane

Another common approach for production of sieves is to directly fabricate sieves inside a microchip. Fan et al.[77] reported a novel PDMS membrane filtration mimic (holes with diameter 6.9–10.8 μm) for fast and effective separation of circulating tumor cells from peripheral blood. As can be seen in Fig. 3a, the PDMS membrane is inserted between the top and bottom chambers with a sacrificial transferring film on top chamber using a sandwich molding method. They
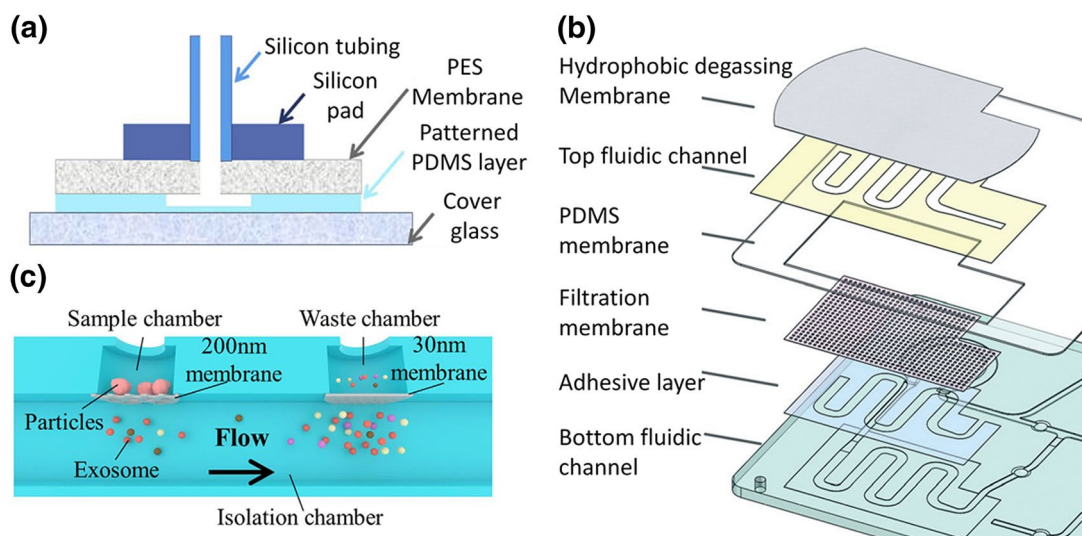

Figure 2: Insertion of membrane on-chip. **a** A schematic of the microfluidic device integrated with a PES membrane sandwiched between PDMS layer and Si substrate[44]. (Copyright 2017, reproduced with permission from Elsevier). **b** Schematic of layer sequence starting from bottom to top: bottom fluidic channel layer, an adhesive layer, filtration membrane layer, PDMS layer, a top fluidic channel layer, hydrophobic degassing membrane layer[43]. (Copyright 2016, reproduced with permission from Royal Society of Chemistry). **c** Schematic of a double-filtration microfluidic device isolating extracellular vesicles with a size between 30 and 200 nm based on particle size exclusion[111]. (Copyright 2017, reproduced with permission from Nature Publishing Group).
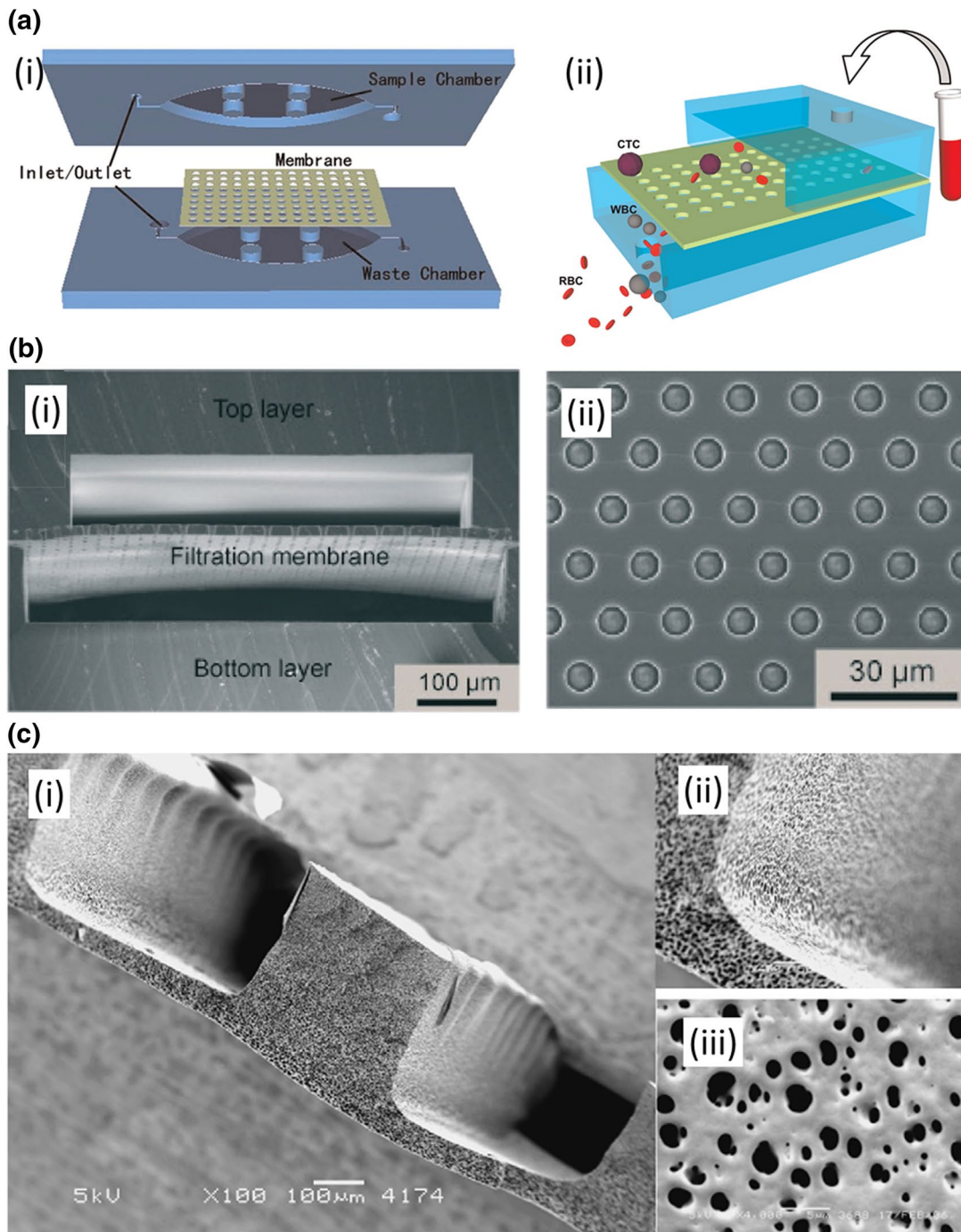
Figure 3: Sieves made of the permeable membrane. **a** (i) A sectional view and (ii) a side view of the microfluidic device integrated with PDMS microfiltration membrane (PMM) with a regular array of holes of diameter 6.9–10.8 μm capturing > 90% of circulating tumor cells from peripheral blood[77]. (Copyright 2015, reproduced with permission from Elsevier). **b** (i) Cross-sectional SEM image showing a PMM sandwiched between the top and bottom PDMS layers. (ii) A top view of PMM membrane containing a hexagonal array of holes with a pore diameter of 4 μm, a pore centre-to-centre distance of 12 μm and a thickness of 10 μm[78]. (Copyright 2014, reproduced with permission from Royal Society of Chemistry). **c** (i) Cross-sectional SEM image of a microfluidic membrane chip with the channel and active membrane, (ii) SEM images show the uniformity of pores and (iii) SEM image shows the membrane surface[68]. (Copyright 2010, reproduced with permission from Elsevier).

143

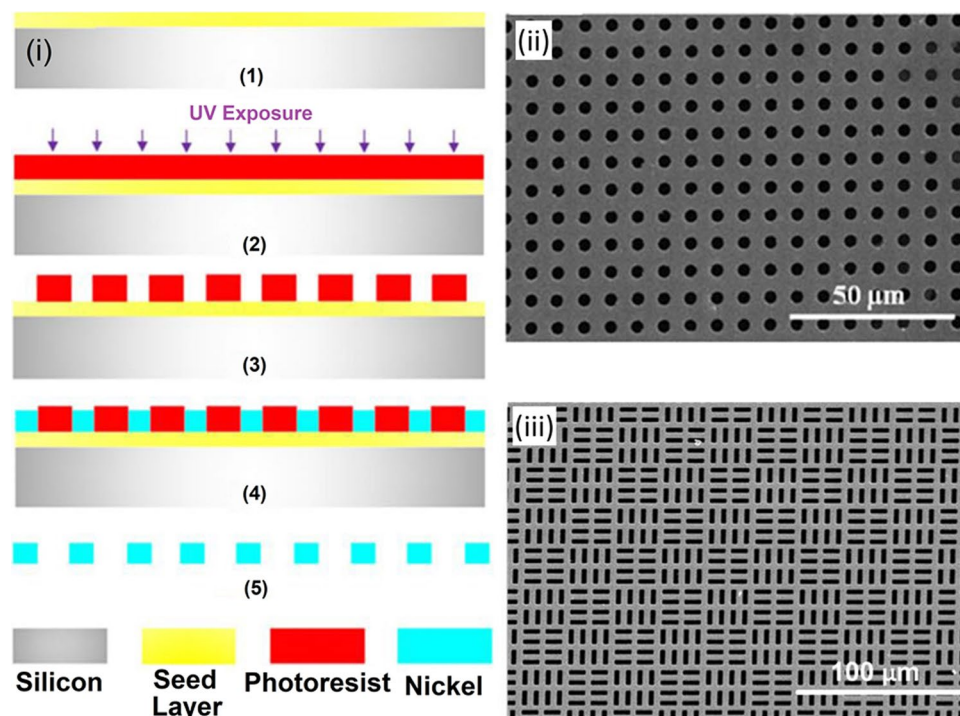J. Indian Inst. Sci. |VOL 98:2|137–157 June 2018|journal.iisc.ernet.in

Figure 4: Sieves made of impermeable membrane. (i) Microfabrication steps for the isopore membrane: (1) deposition of the seed layer (Cr/Cu) on a Si substrate, (2) spin-coating of a thick layer on the Si wafer and UV exposure through a mask, (3) development of the exposed film inside a developer, (4) electroplating of the Ni between photoresist pillars, and (5) releasing the isopore membrane by dissolving the photoresist and seed layer in acetone and Cu etchant, respectively. (ii) SEM image of the circular pore membrane with 3 μm diameter and (iii) SEM image of the slotted pore membrane with 3 μm slit width[80]. (Copyright 2015, reproduced with permission from Springer Berlin Heidelberg).

achieved > 90% recovery when separating lung cancer cells from peripheral blood. In another device, Li et al.[78] sandwiched a surface-micromachined PDMS MF membrane with high porosity between a top and a bottom PDMS layers (Fig. 3b) and reported an enhanced permeation performance for the separation of white blood cells (WBCs) from whole blood. With a sample throughput of 1 mL/h, this cross-flow microfluidic filtration assembly recovered 27.4 ± 4.9% of WBCs with a purity of 93.5 ± 0.5%. Ngene et al.[68] observed a local deposition of a cake layer during filtration of polystyrene particles (6 μm) and described a new method for non-invasive in situ fouling characterization. To prepare the embedded channel membrane, first, square silica capillaries were glued to a glass plate with double sided tape. Next, a solution of PEI/PVP/NMP (19/11/70, w/w/w) was cast on a glass plate at room temperature and phase separation technique was used to release the membrane form the glass plate. Next, the membrane was left in the water bath and sodium oxochlorate (4000 ppm)

to completely remove solvent. When the structured membrane was ready, they fused silica capillary in the channels and the membrane with capillary was placed in between lamination sheet for sealing. SEM image of the embedded membrane channel is shown in Fig. 3c.

Leichle et al.[70] discussed a fabrication method to incorporate a Si membrane inside a microchannel and demonstrated a dead-end MF at micron-scale by retaining 300 nm diameter polymer microspheres. De Jong et al.[79] reported Phase Separation Micro Molding method to generate thin polymeric microfluidic devices with tunable porosity. The tunable porosity of the chip materials was achieved using micro-molding phase separation technique offering a specific transport system for gasses, liquids, and solutes.

3.1.3 Direct Casting of Sieves Made of Impermeable Membrane

Chen et al.[81] described a novel fabrication technique to generate a wide range of pore sizes in PDMS MF membranes. They created sieves (4 μm

144

Springer · IISc Press

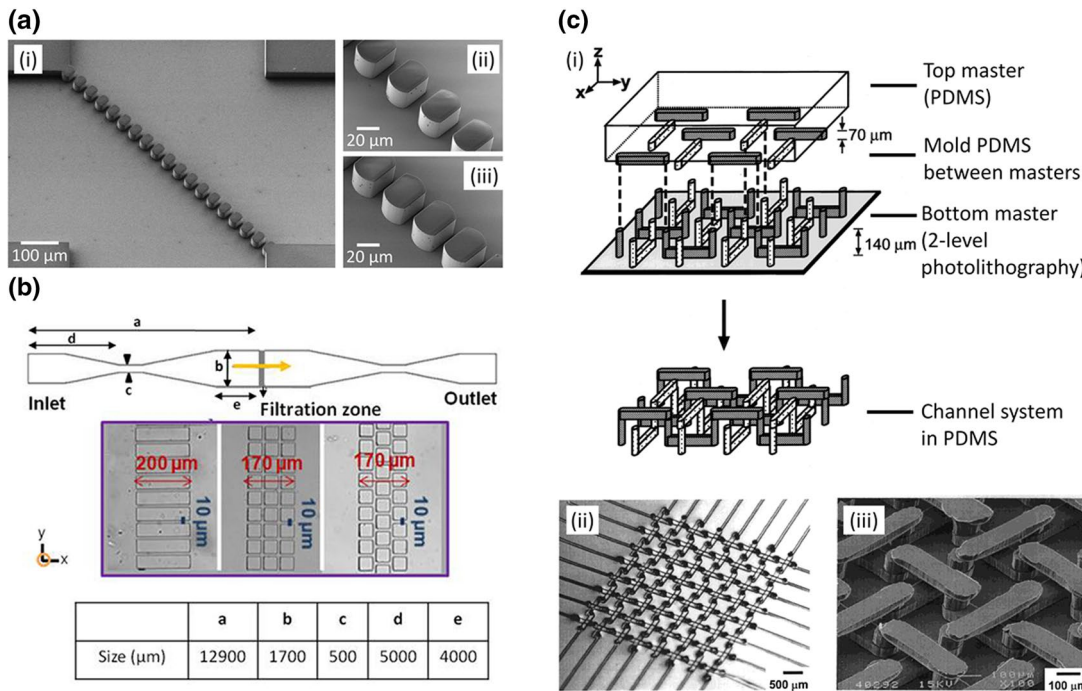J. Indian Inst. Sci.|VOL 98:2|137–157 June 2018|journal.iisc.ernet.in

Figure 5: Pillars or structures made of impermeable membrane. **a** (i) SEM image of a microchannel containing a diagonally aligned single row of pillars (30 μm thick pillars) with pillar gap (ii) 12 μm for sieving PS particles, and (iii) 7 μm for sieving cancer cells from whole blood[85]. (Copyright 2016, reproduced with permission from Nature Publishing Group). **b** Schematic representation of the microfluidic channel working in a dead-end mode with dimensions as shown. The inset details the filtration zone with different micro-channel geometries: straight rectangular, straight squared and staggered squared pillars (from left to right) with 10 μm gap[83]. (Copyright 2014, reproduced with permission from AIP Publishing). **c** A microchannel system fabricated in a basket weave pattern. (i) Schematic of the top and bottom masters resulting in a membrane sandwich. Features in photoresist oriented in the *y*-direction are marked darker than those in the *x*-direction. (ii) The optical image (looking down the *z*-axis) of the PDMS membrane containing 8 × 8 channel system. The channels are 100 μm wide (*x*- or *y*-direction), and each of the three levels used in the fabrication is 70 μm high (*z*-direction) but is not enclosed. (iii) SEM image of the basket weave. It was obtained by filling the microchannel with the epoxy prepolymer, curing under ultraviolet light for 10 min, and dissolving the PDMS casing in tetrabutylammonium fluoride[49]. (Copyright 2000, reproduced with permission from American Chemical Society).

diameter) by photolithography micromachining with PDMS material, where particles passed through the sieves only. Also, they added more layers with plasma bonding between PDMS–PDMS layers. Warkiani et al.[80], fabricated slotted and circular isoporous microfluidic membranes (Fig. 4) by photolithography and electroplating. They found that membrane pore geometry played a significant role in flux decline without a sacrifice in selectivity. In another study, Metz et al.[61] developed a polyamide microfluidic device with nanoporous filtration areas by micromachining and ion track technology to generate microfluidic channel and sieves, respectively. The cross-sectional SEM images of the channel with sieves revealed perforation of only the top layer when the microfluidic channel was irradiated

with ions of low energy and both layers when it was irradiated with ions of high energy.

The general advantage for the sieve method includes the flexible choice of membrane materials with the required pore size for specific application. For example, these devices can be used for selective separation and sensitive detection of an element from a mixture. Another advantage is that during filtration, sometimes, unwanted air bubbles are trapped inside a microfluidic device. Cheng et al.[43] reported a bubble and clogging free microfluidic device by incorporating a degassing membrane at the top of the membrane microchip assembly as shown in Fig. 2b. Liu et al.[110] discovered a novel, simple, nozzle-type, membrane-based debubbler that can be readily integrated with a microfluidic channel for complete

J. Indian Inst. Sci. |VOL 98:2|137–157 June 2018|journal.iisc.ernet.in

Springer   IISc Press

145

degassing and to avoid the formation of air bubbles inside a microchannel.

The most prominent challenge for the robust application of this method is the problem with sealing. To ensure sealing in a microfluidic membrane system clamping or stamping[53, 67], lamination sheets[68] and crosslinking agents[43, 54] have been used so far.

3.2 Production of an Array of Pillars or Structures

In this section, the production of an array of pillars or structures used as on-chip membrane pores is reviewed. Microfluidic PDMS microchips are fabricated with an array of narrow parallel pillars or micro posts, enabling a "side view" of the pores, which is complementary to the top view obtained in the membrane filtration studies using micro-sieves discussed earlier[15, 73, 74, 76–78, 82, 111]. The side view is important to observe the developing thickness of a fouling layer on a membrane surface.

Peterson[112] critically reviewed solid supports for micro-analytical systems including microchips with beads, incorporating membranes into chips, creating supports using microfabrication, fabricating gels and polymer monoliths within microfluidic channels. Gossett et al.[93] reviewed and designed weir-type, pillar type, and crossflow type microscale filters. Yoon et al.[85] and Devendra et al.[91] developed a clog-free microfluidic filtration device by creating a single pillar row for micro-particle separation in a continuous operation. The SEM image of a single row of pillars is shown in Fig. 5a[85]. A similar study was done by Chen et al.[82] with two consecutive PDMS pillar rows that was utilized for blood cell separation application. Chen et al.[50] used a dissolving mold technique to fabricate dissolvable polymeric pillar membranes. Marty et al.[83] studied the impact of tortuosity on bacterial streamer formation by fabricating straight and staggered square arrays of pillars, as shown in Fig. 5b. A similar study was done by Biswas et al.[86] with circular pillar arrangement to investigate the dynamics of bacterial streamer in a microfluidic system. Figure 5c shows a complex microfluidic system with asymmetric PDMS microchannel[49].

Chen et al.[82] and Alvankarian et al.[87] designed cross-flow micro-separators for the separation of plasma and blood cells from human blood based on size-exclusion mechanism. The most significant advantage of this kind of device is that it enables the use of specific channel geometries. Also, as mentioned before, the side view of the pore adds significant value to the fouling investigations, which is not possible in sieve method.

3.3 Membrane-Less Filtration

Here we refer to the filtration methods where separation is based on inertial flow, solute gradient, liquid membrane formation by two-phase or multi-phase flow, and the production of lipid bilayer in a microfluidic device. For example, Seo et al.[94] and Warkiani et al.[96] reported inertial migration in a microfluidic device resulting in membrane-free MF, thus eliminating the need for filter replacement and external force. They introduced curvilinearity to the channel design where the equilibrium position of the particles depends on the balance between shear induced and wall induced lift force and drag force. Thus, two-counter rotating vortices in the top and bottom half of the channel (i.e., Dean vortices) were generated and majority of the particles was trapped on the outer wall, facilitating the filtration. Shin et al.[95] developed membrane-less water filtration techniques by exposing negatively charged suspended particles (polystyrene, diameter ∼ 0.5 mm, zeta potential ∼ − 70 mV) to CO_2. Due to the dissolution of CO_2 into the suspension, large diffusion potential was generated by the dissociation of carbonic acid. Thus, a solute gradient was generated which drove the phoretic motion of the suspension either away from or towards the gas–liquid interface depending on the surface charge.

Another membrane-less filtration is the generation of a liquid membrane inside a microchip by two-phase, three-phase or multiphase flow. By two-phase flow, SooHoo and Walker[98], separated leukocytes when whole blood cells were simultaneously exposed to polyethylene glycol and dextran phase streams. The cells were separated based on their differential affinity for the streams[98]. Maruyama et al.[99] and Surmeian et al.[101], created liquid membrane by three-phase flow through a micro-chip to isolate metal ions and to investigate molecular transport, respectively. Sato et al.[100] reviewed chemical and biochemical analysis systems using microfluidic devices for multi-phase flow liquid membrane production.

Lastly, the membrane-less microfiltration can be explored for the production of lipid bilayers. A model lipid bilayer comprised of single or multiple component lipids[102]. A lipid bilayer formation can last for 2–3 days allowing the robust characterisation of the same lipid membrane[102, 103]. Malmstadt et al.[104] developed a self-assembled lipid bilayer structure driven by a solvent extraction process in a microfluidic device. Watanabe

et al.[108] reported the formation of more than 10,000 asymmetric on-chip lipid bilayer membranes for pharmacological applications. While a thorough review is beyond the scope of this paper, many studies can be found on artificial lipid membrane technology[105, 106].

4 Microfluidic Colloid Filtration

Colloids have a strong tendency to foul the membrane, considerably decreasing permeate flux and the quality of the filtrate. Numerous efforts have been made to understand the colloidal fouling of membranes by ex situ methods[113, 114]. However, challenges remain for in situ experimental technique to understand hydrodynamic effects, locate particle capture and quantify the physicochemical interactions occurring during colloid membrane filtration at the pore scale. Microfluidic membrane filtration is a breakthrough technology in understanding these fouling phenomena. Microfluidic membrane devices provide a large internal surface area to volume ratio that facilitates studying, analyzing and controlling membrane–colloid, and colloid–colloid physiochemical interactions. Microfluidic membrane mimics are handy tools to conduct a real-time visualization of complex colloidal suspension which causes fouling at the pore scale[37, 48, 68, 80, 83, 115]. Moreover, using a microfluidic device, it is possible to generate a uniform array of pores to start with a simple flow and thus to perform a systematic analysis.

Several factors can affect the fouling behavior in a membrane[8, 9, 113]. A number of studies in the literature have shown that membrane fouling is influenced by the local structure of the membrane, as well as the interplay between the hydrodynamic and complex behavior of feed components and the membrane surface[8, 9, 113, 114, 116]. Based on earlier observations of on-chip microfluidic membrane fouling[44, 90, 115], colloidal fouling mechanisms are classified as: (1) cake layer formation at the upstream (membrane surface); (2) deposit collapse and expulsion, (3) clogging of membrane pores; and (4) colloidal streamer formation at the downstream (permeate side). Table 2 summarizes fouling phenomena observed in microfluidic filtration devices.

4.1 Cake Layer Formation

At the beginning of filtration experiments, suspension stability plays an essential role in the deposition of particles on the membrane surface. Over time, stable arches are formed at the entrance pore, from which valuable information about a balance between hydrodynamic force and interfacial forces can be obtained[117]. Agbangla et al.[118] identified the critical conditions for the formation of arches, leading to deposit formation, in terms of particle concentration, solution velocity, and critical flux. As filtration continues, deposit formation eventually leads to stable cake layer formation. Ngene et al.[68] described a new method for obtaining a side view of the formation of a homogeneous cake layer at the channel entrance by the dead-end filtration of 6 μm polystyrene particles.

During filtration, hydrodynamic effects, particle suspension properties (ionic strength and pH), surface interaction potential, and channel geometry play significant roles in particle capture as listed in Table 2. An experimental study by Bacchin et al.[37, 89, 119] showed two types of fouling phenomena occurring in PDMS MF microfluidic membrane mimics. Latex particles (4.9 ± 0.21 μm) with a negatively charged functional sulfate group were used as suspensions in two surface conditioning of PDMS surface: more hydrophilic surface conditioning by 10^{-1}M KCl and more hydrophobic surface conditioning by ultra-pure water[37]. For ultrapure water conditioning, they observed cake layer formation (Fig. 6a (i)). On the contrary, for a more hydrophilic surface, they observed dendrites formation (Fig. 6a (ii)) after 90 min of filtration. They explained that more hydrophilic KCl conditioning caused lower collision efficiency of particles with the PDMS wall at the microchannel entrance. On the contrary, the formation of arches could be promoted by an efficient lateral collision between the particles and the wall, eventually forming a cake layer for a less hydrophilic surface[37]. From their experimental findings, Derekx et al.[120] claimed that the PDMS microfluidic mimic membrane with a 20 μm pillar gap was prone to fouling by latex particles of 1 to 1.25 μm diameter. Similar cake layer formation was observed by Linkhorst et al.[90]. They observed a colloidal cake layer formation when they infused microgels (2.2 μm diameter) through 20 μm pillar gap under constant flux (Fig. 6b (i))[90]. A longer constant flux filtration resulted in the growth of the cake layer and an increase in the trans-cake pressure drop over time. Eventually, the microgels escaped stress by reorganizing into energetically favorable structures such as larger crystalline regions (Fig. 6b (ii)).

Sendekie et al.[115] showed colloidal surface interactions played a significant role in the permeability at the pore scale. At first, critical flux was determined by a flux stepping experiment. Sulfate-modified polystyrene particles (5 μm)

Table 2: Categorization of colloidal fouling observed in a microfluidic membrane filtration system.

Mechanism	Colloids	Location	Factors affecting this phenomenon
Cake layer formation	Dilute or stable suspensions	Upstream of membrane	*Hydrodynamic conditions*
Deposit collapse, expulsion and pore clogging	Aggregates and flocs	Membrane pore	Flux, crossflow velocity, pressure
Colloidal streamer formation	Concentrated or unstable solution, viscoelastic solution	Downstream of membrane	*Feed solution properties* Foulant type, concentration, pH, ionic strength, the presence of coagulants and flocculants
			Surface interaction Surface charge, surface functional group
			Effect of pore geometry Microchannel entrance geometry Sieve size Gap between pillars

were used under KCl conditioning (0.01, 10, and 100 mM) as clogging material (Fig. 6c). They found that particle capture (fouling rate) was more significant for low flow rates and high ionic strengths. This was because increasing ionic strength reduced electric double layer (EDL) repulsion and lowered the energy barrier for particle–surface interaction (Fig. 6c). Therefore, critical flux increased when repulsive forces were more dominant for colloid–surface interactions of 10 mM KCl solution (Fig. 6c). Bacchin et al.[89] experimentally demonstrated the effects of channel connectivity and tortuosity on the particle capture using a straight rectangular microchannel, and a straight and staggered array of square pillars in PDMS microchip. They concluded that the progressive capture of particles occurs on the internal layers as tortuosity increases. Later on, the pore plugging progressed toward the upstream, blocked the channel entrance, and led to the formation of a cake layer. In addition, greater particle deposition on the surface of the square pillars was observed when the pillars were staggered. The increase in clogging by increasing the tortuosity was attributed to the presence of more flow stagnation zones[115]. Sendekie et al.[115] investigated the effect of microchannel entrance geometry on permeation and fouling properties (Fig. 6d). In Fig. 6d, D denotes dead-end flow, S and T denote square and tilted pillars, respectively, and 10 represents pillar gap with 10 μm dimension. Permeability loss was more severe for tilted funneling entrance (DT10) compared to the square entrance (DS10) though greater particle deposition was observed for DS10. This was because the square geometry resulted in a larger flow stagnation area[115], which was in good

agreement with the classical CFT[121]. From Fig. 6d (iii), they attributed the higher flux decline for DT10 to pore clogging phenomenon and less flux decline for DS 10 to more cake layer formation.

4.2 Deposit Collapse, Expulsion and Pore Clogging

Cake layer formation and pore-clogging can be reversible through collapse and expulsion of deposited particles or aggregates. When the flow velocity over adhered particles, or the hydrodynamic forces exceed the repulsive surface interaction force (due to particle–particle and particle–surface interaction), the aggregate begins to collapse or sliding off the walls to the pore[115]. As a consequence, it can substantially affect the permeation flow rate. A similar collapse of the cake layer was observed in membrane filtration by other researchers[122, 123].

During colloidal fouling, colloidal particles aggregate, coagulate, flocculate and begin to plug the membrane pores. Pore-clogging results from progressive particle accumulation, as the pores begin to narrow with the formation of more robust flocs or stable arches. Fouling can be a result of all the factors listed in Table 2, and hydrodynamic effects can be altered due to pore clogging. The process of pore-clogging continues until all pores are blocked, resulting in a significant drop in permeability for constant pressure filtration, and pressure build-up for constant flux filtration. Sendekie et al.[115] made a significant observation of these phenomena from a microfluidic experiment. Figure 7a shows pore-clogging downstream of pillars for a 10 mM KCl solution. They reported the presence of a
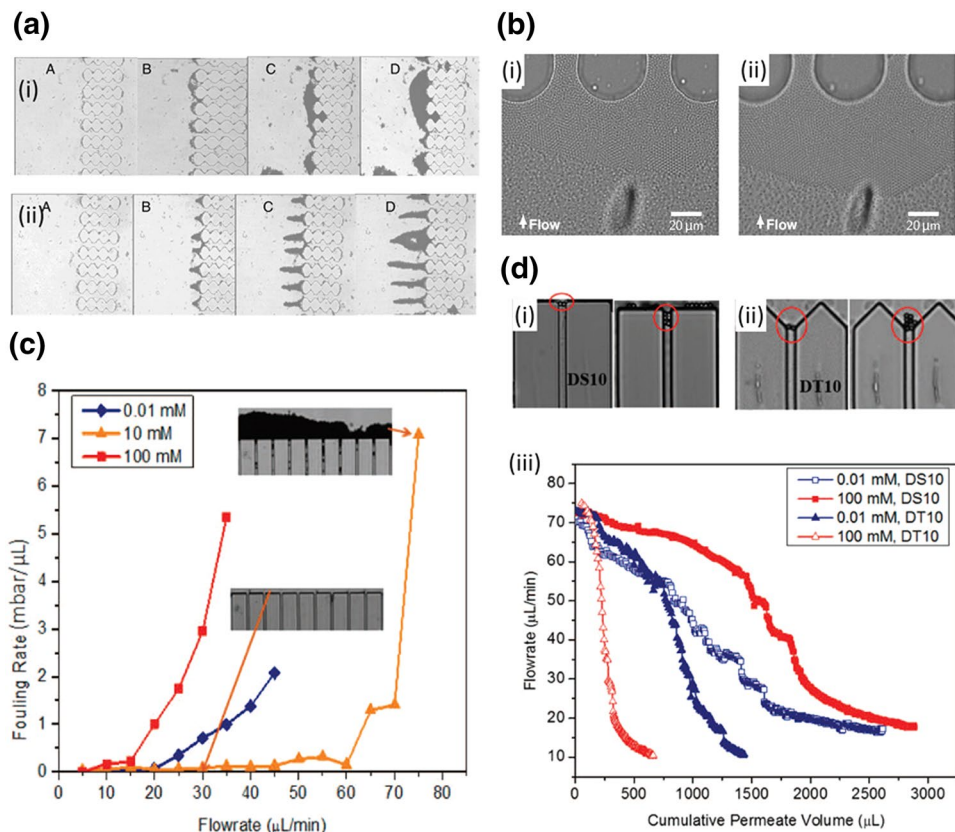
Figure 6: a Microfluidic observation of cake layer formation: microfluidic images showing stable cake layer formation with time for 20 μm pillar gap for (i) ultrapure water conditioning and (ii) KCl solution conditioning of PDMS surface[37]. (Copyright 2011, reproduced with permission from Elsevier). **b** (i) The build-up of the cake layer during filtration of microgel suspension and (ii) increasing pressure increases crystallinity[90]. (Copyright 2016, reproduced with permission from Nature Publishing Group). **c** Effects of ionic strength: fouling rates calculated from the flow stepping experiments at different solution ionic strengths: 0.01, 10 and 100 mM of KCl. The inset images are the observations for 10 mM suspensions before and after deposit formation, and **d** effect of entrance geometry on flow rate and fouling with square entrance (DS10) and tilted funnel entrance (DT10). Filtration results were at constant pressure (200 mbar) for low (0.01 mM) and high ionic strength (100 mM) of KCl demonstrating higher flux decline for DT10. D denotes dead-end flow, S and T denote square and tilted pillars, respectively, and 10 is the channel width[115]. (Copyright 2016, reproduced with permission from American Chemical Society).

secondary energy minimum for a 10 mM KCl solution along with the moderate colloid–surface repulsion at the channel gap. As a result, fluid drag force and shear, dragged particles along the pore wall until they reach the stagnation point in the downstream of pillars (Fig. 7b).

Sendekie and Bacchin[115] also successfully demonstrated the dynamics of pore-clogging with a reasonable relation to an energy barrier. Based on their study, three clogging scenarios can be observed: the panic; the herding instinct; and the sacrifice. Figure 7b summarizes clogging dynamics based on variations in the ionic concentration of KCl. Considering colloid–colloid and colloid–surface interactions, as well as the deposit

structure, specific resistance, and relaxation property, they explained the scenarios mentioned above. First, high repulsive barriers for 0.01 mM KCl caused force chains that sustained the clogs and thus has led to the formation of dense arches (the panic). Second, a significant secondary minimum at 10 mM KCl caused coordinated transport where a pulling effect caused by attraction forces between particles enabled the transfer of the clusters through the bottleneck and delayed the clog formation (the hardening instinct). Third, the low repulsive barrier at 100 mM KCl caused a high collision frequency, leading to the attachment of particles to the walls and the formation of fragile clogs (the sacrifice)[115].

Springer · IISc Press

4.3 Streamer Formation

Colloidal fouling in a porous media can lead to streamer formation at the downstream pores[124, 125]. Here, the term colloidal fouling can be generalized for biofouling and non-biological colloidal fouling. Biofouling occurs when streamers, filamentous structure containing bacterial cells encapsulated in a biopolymer matrix called extra-cellular polymeric substances (EPS)[126], are usually formed in hydrodynamic flow condition[127, 128]. The formation of bacterial streamers can significantly affect fouling of the filtration unit and lower its performance[83, 86, 129]. What's more, medical devices are prone to biofouling due to streamer formation[127, 130]. Biswas et al.[86] studied the deformation mechanism of bacterial streamer occurring at the downstream location of micro-pillars arranged in a staggered pattern (pillar gap 10 µm) (Fig. 8a). Marty et al.[83, 124] fabricated microfluidic membrane mimic with dead-end and cross-flow filtration modes to observe physical processes governing biofouling. Direct observation of bacterial streamer formation was conducted downstream of the pillars (pillar gap 10 or 20 µm) using *E. coli*, *P. aeruginosa*, and *S. aureus* bacterial suspensions. 200 µm long streamer grew after an hour, filtration experiment. Streamer growth and morphology was found to be influenced by the geometry of the device. Streamer were longest for the staggered arrangement of square pillars[124].

Streamer can be non-biological. Debnath et al.[125] reported abiotic or colloidal streamer formation due to a combined flow of poly-acrylamide (PAM) solution and polystyrene (PS) particles into a microfluidic device (Fig. 8b). To show a direct relationship between hydrodynamics and streamer formation, they demonstrated the flow regime through a phase diagram. They concluded that flocculation of PS beads had a significant impact on streamer formation.

5 Strengths and Limitations

Several challenges in understanding the transport and fouling mechanisms in porous membranes can be overcome using a microfluidic membrane filtration system. The general advantages of a microfluidic device include saving time, space, material and cost, better control of flow, and high-throughput. Microfluidic membrane filtration devices, with the flexible design of the microchips, can be utilized for separation, purification and concentration studies at micron-scale. Microfluidic membrane chips enable creating defect-free porous surfaces with homogeneous properties that can be operated in a continuous and uniform-flow filtration process. These devices are highly efficient as one can have more control over the time, size, and experimental parameters, as well as, the flow hydrodynamics. Given that, these devices have been used for many industrial applications to improve separation efficiency and material properties.

To fabricate a microfluidic membrane filtration system the selection of proper material for the intended application is critical. Several studies have shown promising results using PDMS microfluidic membranes in colloid filtration and fouling investigations, as discussed earlier.
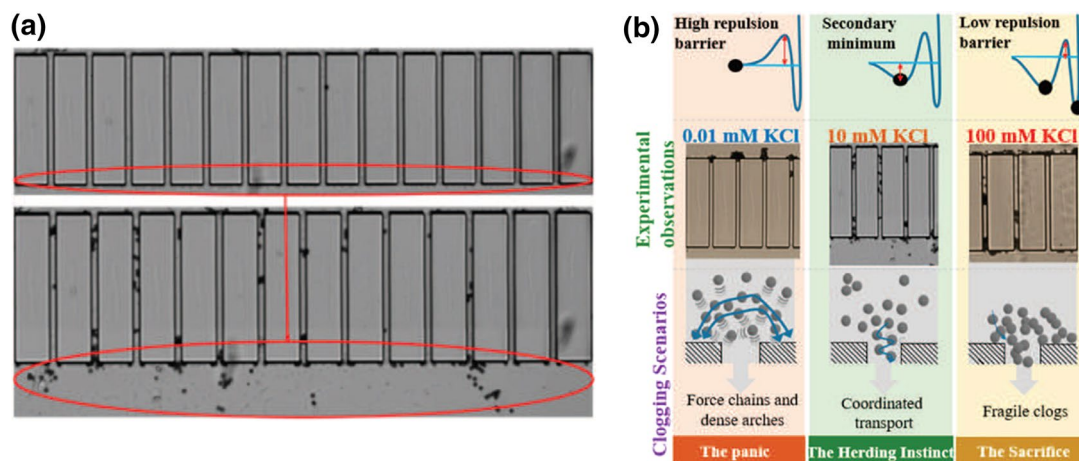

Figure 7: a Observation of pore-clogging for 10 mM KCl solution at the downstream of pillars[115]. **b** Demonstration of the link between DLVO theories, the experimental results, and the clogging scenarios[115]. (Copyright 2016, reproduced with permission from American Chemical Society).

150

Springer · IISc Press

J. Indian Inst. Sci.|VOL 98:2|137–157 June 2018|journal.iisc.ernet.in

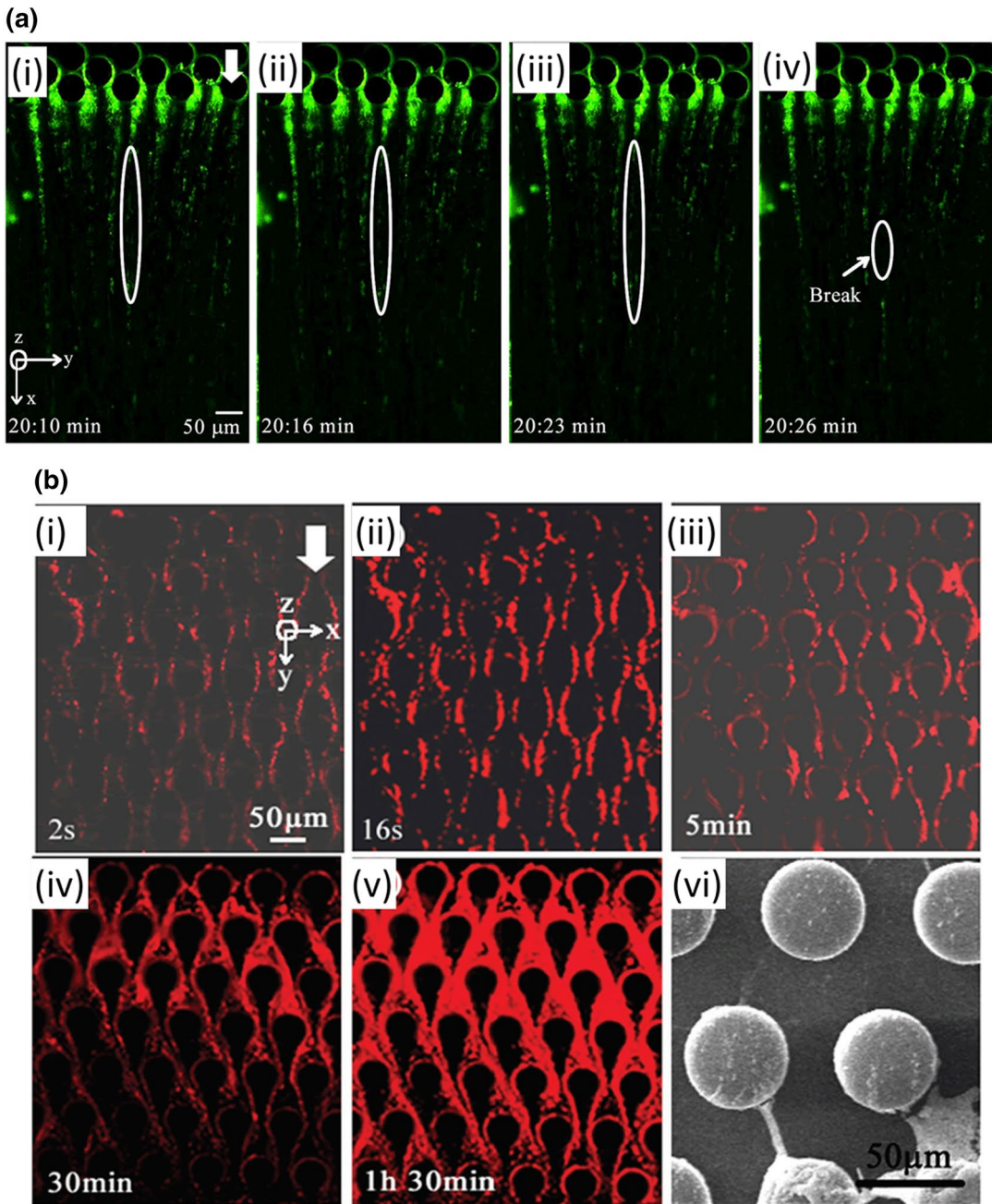Figure 8: **a** Bacterial streamer formation and breaking with time (*P. fluorescens*) under fluorescence imaging with green filter cube at U=8.92×10⁻⁴ m/s. (i–iv) Show the stretching of one streamer with time, and final breaking point shows in (iv). The arrow is showing the flow direction[86]. (Copyright 2016, reproduced with permission from Nature Publishing Group). **b** Abiotic streamer formation in a microfluidic device with time. (i–iii) the viscous streamer formation for a short period and (iv–v) the elastic streamer formation with time and (vi) SEM image of the colloidal streamer inside micro-chip[125]. (Copyright 2017, reproduced with permission from Royal Society of Chemistry).

The PDMS microchip has several advantages such as low toxicity, elasticity, chemical inertness, strong gas permeability, and low cost. The use of a PDMS microchip is, however, limited by the aging of material, poor chemical compatibility, the absorbance of small molecules and water vapor generation inside a microchip.

Several challenges and limitations can be encountered using microfluidic colloid membrane filtration. The first and foremost challenge is the fabrication of microchips with the scaling

comparable with the pores of typical porous membranes. The conventional photolithography technique, as the most common microfabrication method, can be employed for the fabrication of the smallest feature sizes of 0.5 µm. This size range is highly comparable to an MF membrane pore size (0.1–10 µm). E-beam photolithography techniques can go down to 10 nm as the smallest feature size, but it is more expensive than microfabrication. Therefore, new process techniques are required to fill the gap between the properties of a microfluidic membrane and a real membrane.

Another major challenge of using a microfluidic device is its inability to capture the effect of concentration polarization on permeation and fouling properties. Although it is possible to visualize the cake layer formation, however, as most of the solutes are not retained due to the large pore size, it barely gives insight into the concentration polarization phenomenon.

Microfluidic membrane mimic can be used to study biofouling. However, the dynamic nature and the viscoelastic behavior of the active components like bacteria, make the analysis more complicated. Hence, the efficiency of this system needs to be fully understood, especially, in the case of soft, deformable and permeable colloids.

6 Summary and Future Trends

In this review, an outline of the connections between membrane technology and microfluidics has been provided. A special focus is made on the application of microfluidic membrane filtration devices for investigating the colloidal fouling. Applying a massive variety of fabrication methods, microfluidic membrane filtration devices can be scalable and designed for specific applications, such as separation of colloids, organic matter, and biological substances from wastewaters. Furthermore, using a microfluidic membrane filtration device, the internal surface can be exploited for investigating the fouling dynamics and morphology, intermolecular interactions, and transport mechanisms at the pore scale.

Microfluidic membrane filtration device opens up many future opportunities. This device can be used as a model system to investigate certain phenomena under physiologically significant conditions that are limited by traditional filtration techniques. For example, microfluidic device has been used to mimic components of the liver[131], lung[132], and heart[133, 134]. Microfluidic membrane mimic may offer key micro-environmental conditions revealing more information about organ functions[135] and vascular circulations[136]. Thus, microfluidic membrane mimic can serve as an ideal model system for future biomedical research.

Another example would be to utilise the benefit of selectivity of a membrane on-chip. As compared to the conventional filtration processes, a microfluidic membrane mimic better protects the microchannel from particulate matter, reduces the unwanted hydrodynamic flow and has more control over sample volume. This device may offer selective separation of liquids in pervaporation, selective removal of one component from a gas mixture, which further needs to be investigated.

Lastly, the membrane-less MF can be explored in many aspects. For example, lipid bilayers production was limited to the fabrication in an array format, which can be further explored for pillar shape or different geometry. In addition, future work is clearly required to achieve quantitative description of lipid bilayer formation process and the role of media compositions.

In conclusion, microfluidic membrane mimic provides a model platform that can add benefits to the microfluidic research from membrane perspective and vice versa through making a bridge between microfluidics and membrane technology.

References

1. Montgomery MA, Elimelech M (2007) Water and sanitation in developing countries: including health in the equation—millions suffer from preventable illnesses and die every year. Environ Sci Technol 41:17–24
2. Shannon MA, Bohn PW, Elimelech M, Georgiadis JG, Marĩas BJ, Mayes AM (2008) Science and technology for water purification in the coming decades. Nature 452:301–310
3. Sadrzadeh M, Hajinasiri J, Bhattacharjee S, Pernitsky D (2015) Nanofiltration of oil sands boiler feed water: effect of pH on water flux and organic and dissolved solid rejection. Sep Purif Technol 141:339–353

152

Springer   IISc Press

J. Indian Inst. Sci.|VOL 98:2|137–157 June 2018|journal.iisc.ernet.in

4. Le NL, Nunes SP (2016) Materials and membrane technologies for water and energy sustainability. Sustain Mater Technol 7:1–28

5. Wiesner MR, Hackney J, Sethi S, Jacangelo JG, Jacangelo JG, Lafne J (1994) Cost estimates for membrane filtration and conventional treatment for membrane filtration and conventional treatment alternative for the removal of particles and organic material. Am Water Works Assoc 86:33–41

6. Baker RW (2012) Membrane technology and applications, 3rd edn. Wiley, West Sussex, pp 1–574

7. Mulder M (1996) Basic principles of membrane technology, 2nd edn. Kluwer Academic Publishers, Dordrecht, pp 1–564

8. Guo W, Ngo HH, Li J (2012) A mini-review on membrane fouling. Bioresour Technol 122:27–34

9. Al Mamun MA, Sadrzadeh M, Chatterjee R, Bhattacharjee S, De S (2015) Colloidal fouling of nanofiltration membranes: a novel transient electrokinetic model and experimental study. Chem Eng Sci 138:153–163

10. Chen V, Fane AG, Madaeni S, Wenten IG (1997) Particle deposition during membrane filtration of colloids: transition between concentration polarization and cake formation. J Membr Sci 125:109–122

11. Mark D, Haeberle S, Roth G, Von Stetten F, Zengerle R (2010) Microfluidic lab-on-a-chip platforms: requirements, characteristics and applications. NATO Sci Peace Secur Series A 39:305–376

12. Haeberle S, Mark D, Von Stetten F, Zengerle R (2012) Microfluidic platforms for lab-on-a-chip applications. Microsyst Nanotechnol 9783642182:853–895

13. Salafi T, Zeming KK, Zhang Y (2017) Advancements in microfluidics for nanoparticle separation. Lab Chip 17:11–33

14. Alvankarian J, Majlis BY (2015) Tunable microfluidic devices for hydrodynamic fractionation of cells and beads: a review. Sensors (Switzerland) 15:29685–29701

15. Ng E, Chen K, Hang A, Syed A, Zhang JXJ (2016) Multidimensional nanostructures for microfluidic screening of biomarkers: from molecular separation to cancer cell detection. Ann Biomed Eng 44:847–862

16. Gruber P, Marques MPC, Szita N, Mayr T (2017) Integration and application of optical chemical sensors in microbioreactors. Lab Chip 17:2693–2712

17. Hugh Fan Z (2013) Chemical sensors and microfluidics. J Biosens Bioelectron 4:1–2

18. Anema SG (2009) The use of "lab-on-a-chip" microfluidic SDS electrophoresis technology for the separation and quantification of milk proteins. Int Dairy J 19:198–204

19. Dorfman KD, King SB, Olson DW, Thomas JDP, Tree DR (2013) Beyond gel electrophoresis: microfluidic separations, fluorescence burst analysis, and DNA stretching. Chem Rev 113:2584–2667

20. Tsai JH, Lin L (2002) A thermal-bubble-actuated micronozzle-diffuser pump. J Microelectromech Syst 11:665–671

21. Zhang C, Xing D, Li Y (2007) Micropumps, microvalves, and micromixers within PCR microfluidic chips: advances and trends. Biotechnol Adv 25:483–514

22. Ren K, Dai W, Zhou J, Su J, Wu H (2011) Whole-Teflon microfluidic chips. Proc Natl Acad Sci 108:8162–8166

23. Horsman KM, Bienvenue JM, Blasier KR, Landers JP (2007) Forensic DNA analysis on microfluidic devices: a review. J Forensic Sci 52:784–799

24. Khandurina J, McKnight TE, Jacobson SC, Waters LC, Foote RS, Ramsey JM (2000) Integrated system for rapid PCR-based DNA analysis in microfluidic devices. Anal Chem 72:2995–3000

25. Chen X, Shen J, Hu Z, Huo X (2016) Manufacturing methods and applications of membranes in microfluidics. Biomed Microdevices 18:104

26. de Jong J, Lammertink RGH, Wessling M (2006) Membranes and microfluidics: a review. Lab Chip 6:1125

27. Chen X, Shen J (2017) Review of membranes in microfluidics. J Chem Technol Biotechnol 92:271–282

28. Sackmann EK, Fulton AL, Beebe DJ (2014) The present and future role of microfluidics in biomedical research. Nature 507:181–189

29. Chiu DT, de Mello AJ, Di Carlo D, Doyle PS, Hansen C, Maceiczyk RM, Wootton RCR (2017) Small but perfectly formed successes, challenges, and opportunities for microfluidics in the chemical and biological sciences. Chem 2:201–223

30. Zhang J, Yan S, Yuan D, Alici G, Nguyen N-T, Ebrahimi Warkiani M, Li W (2016) Fundamentals and applications of inertial microfluidics: a review. Lab Chip 16:10–34

31. Ng JMK, Gitlin I, Stroock AD, Whitesides GM (2002) Components for integrated poly(dimethylsiloxane) microfluidic systems. Electrophoresis 23:3461–3473

32. Stroock AD, Whitesides GM (2002) Components for integrated poly (dimethylsiloxane) microfluidic systems. Electrophoresis 23:3461–3473

33. Mou L, Jiang X (2017) Materials for microfluidic immunoassays: a review. Adv Healthcare Mater 6:1–20

34. Bruus H (2008) Theoretical microfluidics. Physics 18:1–237

35. Iliescu C, Taylor H, Avram M, Miao J, Franssila S (2012) A practical guide for the fabrication of microfluidic devices using glass and silicon. Biomicrofluidics 6:16505–1650516

36. Likos C (2001) Effective interactions in soft condensed matter physics. Phys Rep 348:267–439

37. Bacchin P, Marty A, Duru P, Meireles M, Aimar P (2011) Colloidal surface interactions and membrane fouling: Investigations at pore scale. Adv Coll Interface Sci 164:2–11

38. Yao KM, Habibian MT, O'Melia CR (1971) Water and waste water filtration: concepts and applications. Environ Sci Technol 5:1105–1112

39. Tufenkji N, Elimelech M (2005) Breakdown of colloid filtration theory: role of the secondary energy minimum and surface charge heterogeneities. Langmuir 21:841–852

40. Tufenkji N, Elimelech M (2004) Deviation from the classical colloid filtration theory in the presence of repulsive DLVO interactions. Langmuir 20:10818–10828

41. Hoek EMV, Bhattacharjee S, Elimelech M (2003) Effect of membrane surface roughness on colloid-membrane DLVO interactions. Langmuir 19:4836–4847

42. Van den Broeck C, Lostak F, Lekkerkerker HNW (1981) The effect of direct interactions on Brownian diffusion. J Chem Phys 74:2006–2010

43. Cheng Y, Wang Y, Ma Z, Wang W, Ye X (2016) A bubble- and clogging-free microfluidic particle separation platform with multi-filtration. Lab Chip 16:4517–4526

44. Di H, Martin GJO, Dunstan DE (2017) A microfluidic system for studying particle deposition during ultrafiltration. J Membr Sci 532:68–75

45. Liang L-G, Kong M-Q, Zhou S, Sheng Y-F, Wang P, Yu T, Inci F, Kuo WP, Li L-J, Demirci U, Wang S (2017) An integrated double-filtration microfluidic device for isolation, enrichment and quantification of urinary extracellular vesicles for detection of bladder cancer. Sci Rep 7:46224

46. Ohira S-I, Toda K (2005) Micro gas analysis system for measurement of atmospheric hydrogen sulfide and sulfur dioxide. Lab Chip 5:1374–1379

47. Sticker D, Rothbauer M, Lechner S, Hehenberger M-T, Ertl P (2015) Multi-layered, membrane-integrated microfluidics based on replica molding of a thiolene epoxy thermoset for organ-on-a-chip applications. Lab Chip 15:4542–4554

48. Wei H, Chueh B, Wu H, Hall EW, Li C, Schirhagl R, Lin J-M, Zare RN (2011) Particle sorting using a porous membrane in a microfluidic device. Lab Chip 11:238–245

49. Anderson JR, Chiu DT, Jackman RJ, Cherniavskaya O, McDonald JC, Wu H, Whitesides SH, Whitesides GM (2000) Fabrication of topologically complex three-dimensional microfluidic systems in PDMS by rapid prototyping. Anal Chem 72:3158–3164

50. Chen L, Warkiani ME, Liu HB, Gong HQ (2010) Polymeric micro-filter manufactured by a dissolving mold technique. J Micromech Microeng 20:075005

51. Sundararajan N, Kim D, Berlin A (2005) Microfluidic operations using deformable polymer membranes fabricated by single layer soft lithography. Lab Chip 5:350–354

52. Xu J, Vaillant R, Attinger D (2010) Use of a porous membrane for gas bubble removal in microfluidic channels: physical mechanisms and design criteria. Microfluid Nanofluid 9:765–772

53. Chueh BH, Huh D, Kyrtsos CR, Houssin T, Futai N, Takayama S (2007) Leakage-free bonding of porous membranes into layered microfluidic array systems. Anal Chem 79:3504–3508

54. Pham MH, Barz DPJ (2017) Bonding Nafion® with polydimethylsiloxane: a versatile approach towards ion-exchange membrane microfluidic devices. J Membr Sci 537:310–314

55. Russo AP, Retterer ST, Spence AJ, Isaacson MS, Lepak LA, Spencer MG, Martin DL, MacColl R, Turner JN (2004) Direct casting of polymer membranes into microfluidic devices. Sep Sci Technol 39:2515–2530

56. Thorslund S, Klett O, Nikolajeff F, Markides K, Bergquist J (2006) A hybrid poly(dimethylsiloxane) microsystem for on-chip whole blood filtration optimized for steroid screening. Biomed Microdevice 8:73–79

57. Feng S, Nguyen MN, Inglis DW (2017) Microfluidic droplet extraction by hydrophilic membrane. Micromachines 8:1–8

58. Jiang Y, Lee CS (2001) On-line coupling of micro-enzyme reactor with micro-membrane chromatography for protein digestion, peptide separation, and protein identification using electrospray ionization mass spectrometry. J Chromatogr A 924:315–322

59. Gao J, Xu J, Locascio LE, Lee CS (2001) Integrated microfluidic system enabling protein digestion, peptide separation, and protein identification. Anal Chem 73:2648–2655

60. Cai ZX, Fang Q, Chen HW, Fang ZL (2006) A microfluidic chip based liquid–liquid extraction system with microporous membrane. Anal Chim Acta 556:151–156

61. Metz S, Trautmann C, Bertsch A, Renaud P (2004) Polyimide microfluidic devices with integrated nanoporous filtration areas manufactured by micromachining and ion track technology. J Micromech Microeng 14:324–331

62. Noblitt SD, Kraly JR, VanBuren JM, Hering SV, Collett JL, Henry CS (2007) Integrated membrane filters for minimizing hydrodynamic flow and filtering in microfluidic devices. Anal Chem 79:6249–6254

63. Wang PC, Gao J, Lee CS (2002) High-resolution chiral separation using microfluidics-based membrane chromatography. J Chromatogr A 942:115–122

64. Davies RT, Kim J, Jang SC, Choi E-J, Gho YS, Park J (2012) Microfluidic filtration system to isolate extracellular vesicles from blood. Lab Chip 12:5202–5210

65. Hylton K, Mitra S (2008) A microfluidic hollow fiber membrane extractor for arsenic(V) detection. Anal Chim Acta 607:45–49

66. Paustian JS, Azevedo RN, Lundin STB, Gilkey MJ, Squires TM (2014) Microfluidic microdialysis: spatiotemporal control over solution microenvironments

154

Springer · IISc Press

J. Indian Inst. Sci.|VOL 98:2|137–157 June 2018|journal.iisc.ernet.in

using integrated hydrogel membrane microwindows. Phys Rev X 3:1–13

67. Choi E, Park J (2011) In-situ formation of hydrogel membranes and growth of colloidal crystals in microchannels using one step stamping. In: 15th international conference on miniaturized systems for chemistry and life sciences 2011, MicroTAS 2011, vol 1, pp 236–238

68. Ngene IS, Lammertink RGH, Wessling M, van der Meer W (2010) A microfluidic membrane chip for in situ fouling characterization. J Membr Sci 346:202–207

69. Galambos P, Zavadil K, Shul R, Willison CG, Miller S (1999) Silicon nitride membranes for filtration and separation. Microfluidic Devices Syst II(3877):273–283

70. Leïchlé T, Bourrier D (2015) Integration of lateral porous silicon membranes into planar microfluidics. Lab Chip 15:833–838

71. Chau JLH, Wan YSS, Gavriilidis A, Yeung KL (2002) Incorporating zeolites in microchemical systems. Chem Eng J 88:187–200

72. Vankelecom IFJ, Depre D, De Beukelaer S, Uytterhoeven JB (1995) Influence of zeolites in PDMS membranes. Pervaporation of water/alcohol mixtures. J Phys Chem 99:13193–13197

73. Wan YSS, Chau JLH, Gavriilidis A, Yeung KL (2001) Design and fabrication of zeolite-based microreactors and membrane microseparators. Microporous Mesoporous Mater 42:157–175

74. Toh CS, Kayes BM, Nemanick EJ, Lewis NS (2004) Fabrication of free-standing nanoscale alumina membranes with controllable pore aspect ratios. Nano Lett 4:767–770

75. Bin Liu Z, Zhang Y, Yu JJ, Mak AFT, Li Y, Yang M (2010) A microfluidic chip with poly(ethylene glycol) hydrogel microarray on nanoporous alumina membrane for cell patterning and drug testing. Sens Actuat B 143:776–783

76. Lu Y, Shi W, Qin J, Lin B (2010) Fabrication and characterization of paper-based microfluidics prepared in nitrocellulose membrane by Wax printing. Anal Chem 82:329–335

77. Fan X, Jia C, Yang J, Li G, Mao H, Jin Q, Zhao J (2015) A microfluidic chip integrated with a high-density PDMS-based microfiltration membrane for rapid isolation and detection of circulating tumor cells. Biosens Bioelectron 71:380–386

78. Li X, Chen W, Liu G, Lu W, Fu J (2014) Continuous-flow microfluidic blood cell sorting for unprocessed whole blood using surface-micromachined microfiltration membranes. Lab Chip 14:2565–2575

79. de Jong J, Ankoné B, Lammertink RGH, Wessling M (2005) New replication technique for the fabrication of thin polymeric microfluidic devices with tunable porosity. Lab Chip 5:1240–1247

80. Warkiani ME, Wicaksana F, Fane AG, Gong HQ (2015) Investigation of membrane fouling at the microscale using isopore filters. Microfluid Nanofluid 19:307–315

81. Chen W, Lam RHW, Fu J (2012) Photolithographic surface micromachining of polydimethylsiloxane (PDMS). Lab Chip 12:391–395

82. Chen X, Cui DF, Liu CC, Li H (2008) Microfluidic chip for blood cell separation and collection based on cross-flow filtration. Sens Actuat B 130:216–221

83. Marty A, Causserand C, Roques C, Bacchin P (2014) Impact of tortuous flow on bacteria streamer development in microfluidic system during filtration. Biomicrofluidics 8:1–12

84. Robinson T, Kuhn P, Eyer K, Dittrich PS (2013) Microfluidic trapping of giant unilamellar vesicles to study transport through a membrane pore. Biomicrofluidics 7:044105

85. Yoon Y, Kim S, Lee J, Choi J, Kim RK, Lee SJ, Sul O, Lee SB (2016) Clogging-free microfluidics for continuous size-based separation of microparticles. Sci Rep 6:1–8

86. Biswas I, Ghosh R, Sadrzadeh M, Kumar A (2016) Nonlinear deformation and localized failure of bacterial streamers in creeping flows. Sci Rep 6:2–11

87. Alvankarian J, Bahadorimehr A, Yeop Majlis B (2013) A pillar-based microfilter for isolation of white blood cells on elastomeric substrate. Biomicrofluidics 7:1–16

88. Neeves KB, Diamond SL (2008) A membrane-based microfluidic device for controlling the flux of platelet agonists into flowing blood. Lab Chip 8:701–709

89. Bacchin P, Derekx Q, Veyret D, Glucina K, Moulin P (2014) Clogging of microporous channels networks: role of connectivity and tortuosity. Microfluid Nanofluid 17:85–96

90. Linkhorst J, Beckmann T, Go D, Kuehne AJC, Wessling M (2016) Microfluidic colloid filtration. Sci Rep 6:1–8

91. Devendra R, Drazer G (2014) Deterministic fractionation of binary suspensions moving past a line of microposts. Microfluid Nanofluid 17:519–526

92. Angelescu DE, Mercier B, Sless D, Schroetter R (2010) Microfluidic capillary separation and real-time spectroscopic analysis of specific components from multiphase mixtures. Anal Chem 82:2412–2420

93. Gossett DR, Weaver WM, MacH AJ, Hur SC, Tse HTK, Lee W, Amini H, Di Carlo D (2010) Label-free cell separation and sorting in microfluidic systems. Anal Bioanal Chem 397:3249–3267

94. Seo J, Lean MH, Kole A (2007) Membrane-free microfiltration by asymmetric inertial migration. Appl Phys Lett 91:033901

95. Shin S, Shardt O, Warren PB, Stone HA (2017) Membraneless water filtration using CO_2. Nat Commun 8:1–6

96. Warkiani ME, Tay AKP, Guan G, Han J (2015) Membrane-less microfiltration using inertial microfluidics. Sci Rep 5:1–10

97. Kwon T, Prentice H, De Oliveira J, Madziva N, Warkiani ME, Hamel JFP, Han J (2017) Microfluidic cell retention device for perfusion of mammalian suspension culture. Sci Rep 7:1–11

J. Indian Inst. Sci. |VOL 98:2|137–157 June 2018|journal.iisc.ernet.in

Springer IISc Press

155

98. SooHoo JR, Walker GM (2009) Microfluidic aqueous two phase system for leukocyte concentration from whole blood. Biomed Microdevice 11:323–329

99. Maruyama T, Matsushita H, Uchida JI, Kubota F, Kamiya N, Goto M (2004) Liquid membrane operations in a microfluidic device for separation of metal ions. Anal Chem 76:4495–4500

100. Sato K, Hibara A, Tokeshi M, Hisamoto H, Kitamori T (2003) Microchip-based chemical and biochemical analysis systems. Adv Drug Deliv Rev 55:379–391

101. Surmeian M, Slyadnev MN, Hisamoto H, Hibara A, Uchiyama K, Kitamori T (2002) Three-layer flow membrane system on a microchip for investigation of molecular transport. Anal Chem 74:2014–2020

102. Reviakine I, Brisson A (2000) Formation of supported phospholipid bilayers from unilamellar vesicles investigated by atomic force microscopy. Langmuir 16:1806–1815

103. Hirano-Iwata A, Aoto K, Oshima A, Taira T, Yamaguchi RT, Kimura Y, Niwano M (2010) Free-standing lipid bilayers in silicon chips-membrane stabilization based on microfabricated apertures with a nanometer-scale smoothness. Langmuir 26:1949–1952

104. Malmstadt N, Nash MA, Purnell RF, Schmidt JJ (2006) Automated formation of lipid-bilayer membranes in a microfluidic device. Nano Lett 6:1961–1965

105. Castellana ET, Cremer PS (2006) Solid supported lipid bilayers: from biophysical studies to sensor design. Surf Sci Rep 61:429–444

106. Ota S, Suzuki H, Takeuchi S (2011) Microfluidic lipid membrane formation on microchamber arrays. Lab Chip 11:2485–2487

107. Sandison ME, Morgan H (2005) Rapid fabrication of polymer microfluidic systems for the production of artificial lipid bilayers. J Micromech Microeng 15:S139–S144

108. Watanabe R, Soga N, Yamanaka T, Noji H (2014) High-throughput formation of lipid bilayer membrane arrays with an asymmetric lipid composition. Sci Rep 4:1–6

109. Bacchin P, Aimar P, Sanchez V (1995) Model for colloidal fouling of membranes. AIChE J 41:368–376

110. Liu C, Thompson JA, Bau HH (2011) A membrane-based, high-efficiency, microfluidic debubbler. Lab Chip 11:1688–1693

111. Liang LG, Kong MQ, Zhou S, Sheng YF, Wang P, Yu T, Inci F, Kuo WP, Li LJ, Demirci U, Wang SQ (2017) An integrated double-filtration microfluidic device for isolation, enrichment and quantification of urinary extracellular vesicles for detection of bladder cancer. Sci Rep 7:1–10

112. Peterson DS (2005) Solid supports for micro analytical systems. Lab Chip 5:132–139

113. Tang CY, Chong TH, Fane AG (2011) Colloidal interactions and fouling of NF and RO membranes: a review. Adv Coll Interface Sci 164:126–143

114. Iritani E (2013) A review on modeling of pore-blocking behaviors of membranes during pressurized membrane filtration. Drying Technol 31:146–162

115. Sendekie ZB, Bacchin P (2016) Colloidal jamming dynamics in microchannel bottlenecks. Langmuir 32:1478–1488

116. Ramachandran V, Fogler HS (1998) Multilayer deposition of stable colloidal particles during flow within cylindrical pores. Langmuir 14:4435–4444

117. Sharp KV, Adrian RJ (2005) On flow-blocking particle structures in microtubes. Microfluid Nanofluid 1:376–380

118. Agbangla GC, Climent É, Bacchin P (2012) Experimental investigation of pore clogging by microparticles: evidence for a critical flux density of particle yielding arches and deposits. Sep Purif Technol 101:42–48

119. Bacchin P, Espinasse B, Bessiere Y, Fletcher DF, Aimar P (2006) Numerical simulation of colloidal dispersion filtration: description of critical flux and comparison with experimental results. Desalination 192:74–81

120. Derekx Q, Bacchin P, Veyret D, Glucina K, Moulin P (2012) Numerical and experimental study of fouling in microfluidic channels and microfiltration membranes. Procedia Eng 44:54–56

121. Johnson WP, Hilpert M (2013) Upscaling colloid transport and retention under unfavorable conditions: linking mass transfer to pore and grain topology. Water Resour Res 49:5328–5341

122. Tarabara VV, Koyuncu I, Wiesner MR (2004) Effect of hydrodynamics and solution ionic strength on permeate flux in cross-flow filtration: direct experimental observation of filter cake cross-sections. J Membr Sci 241:65–78

123. Zhang H, Gao J, Jiang T, Gao D, Zhang S, Li H, Yang F (2011) A novel approach to evaluate the permeability of cake layer during cross-flow filtration in the flocculants added membrane bioreactors. Bioresour Technol 102:11121–11131

124. Marty A, Roques C, Causserand C, Bacchin P (2012) Formation of bacterial streamers during filtration in microfluidic systems. Biofouling 28:551–562

125. Debnath N, Hassanpourfard M, Ghosh R, Trivedi J, Thundat T, Sadrzadeh M, Kumar A (2017) Abiotic streamers in a microfluidic system. Soft Matter 13:8698–8705

126. Karimi A, Karig D, Kumar A, Ardekani AM (2015) Interplay of physical mechanisms and biofilm processes: review of microfluidic methods. Lab Chip 15:23–42

127. Valiei A, Kumar A, Mukherjee PP, Liu Y, Thundat T (2012) A web of streamers: biofilm formation in a porous microfluidic device. Lab Chip 12:5133–5137

128. Hassanpourfard M, Nikakhtari Z, Ghosh R, Das S, Thundat T, Liu Y, Kumar A (2015) Bacterial floc mediated rapid streamer formation in creeping flows. Sci Rep 5:1–17

156

Springer · IISc Press

J. Indian Inst. Sci.|VOL 98:2|137–157 June 2018|journal.iisc.ernet.in

129. Hassanpourfard M, Ghosh R, Thundat T, Kumar A (2016) Dynamics of bacterial streamers induced clogging in microfluidic devices. Lab Chip 16:4091–4096

130. Drescher K, Shen Y, Bassler BL, Stone HA (2013) Biofilm streamers cause catastrophic disruption of flow with consequences for environmental and medical systems. Proc Natl Acad Sci USA 110:4345–4350

131. Gori M, Simonelli MC, Giannitelli SM, Businaro L, Trombetta M, Rainer A (2016) Investigating nonalcoholic fatty liver disease in a liver-on-a-chip microfluidic device. PLoS ONE 11:1–15

132. Jiang J, Zhao H, Shu W, Tian J, Huang Y, Song Y, Wang R, Li E, Slamon D, Hou D, Du X, Zhang L, Chen Y, Wang Q (2017) An integrated microfluidic device for rapid and high-sensitivity analysis of circulating tumor cells. Sci Rep 7:1–11

133. Aung A, Bhullar IS, Theprungsirikul J, Davey SK, Lim HL, Chiu YJ, Ma X, Dewan S, Lo YH, McCulloch A, Varghese S (2016) McCulloch, 3D cardiac μ tissues within a microfluidic device with real-time contractile stress readout. Lab Chip 16:153–162

134. Perestrelo AR, Águas ACP, Rainer A, Forte G (2015) Microfluidic organ/body-on-a-chip devices at the convergence of biology and microengineering. Sensors (Switzerland) 15:31142–31170

135. Bhatia SN, Ingber DE (2014) Microfluidic organs-on-chips. Nat Biotechnol 32:760–772

136. Srigunapalan S, Lam C, Wheeler AR, Simmons CA (2011) A microfluidic membrane device to mimic critical components of the vascular microenvironment. Biomicrofluidics 5:1–9

Nandini Debnath received Bachelor's degree in Mechanical Engineering from National Institute of Technoogy, Durgapur, India. Currently, she is a PhD student in the department of mechanical Engineering from University of Alberta. Canada. Her research interest is focused on the microfluidic membrane filtration for colloidal fouling investigations.

Mohtada Sadrzadeh is currently an Assistant Professor in Mechanical Engineering Department at the University of Alberta. He researches the fundamental and applied aspects of membrane materials and process development, focusing on their applications in industrial/residential wastewater treatment.

The contributions made by Dr. Sadrzadeh during his academic career thus far have led to the development and application of novel composite and nanocomposite membranes for water and gas treatment. He is currently directing Advanced Water Research Lab (AWRL) at the University of Alberta that is equipped with the membrane and nanoparticle synthesis and characterization equipment as well as membrane filtration systems. He has an h-index of 28 (according to Google Scholar) with his 70+ refereed publications cited more than 2000 times. He is collaborating with eleven oil and gas companies through Canada's Oil Sands Innovation Alliance (COSIA), IBM, National Research Council (NRC, Canada), Natural Resource Canada (NRCan, Canada) on the synthesis of high-performance membranes.

J. Indian Inst. Sci. |VOL 98:2|137–157 June 2018|journal.iisc.ernet.in

157

⌄ Springer ⓘ IISc Press